Ratios of Charged Antiparticles-to-Particles near Mid-Rapidity in Au + Au Collisions at $\sqrt{s_{NN}} = 130$ GeV

B. B. Back,[1] M. D. Baker,[2] D. S. Barton,[2] R. R. Betts,[1,6] R. Bindel,[7] A. Budzanowski,[3] W. Busza,[4] A. Carroll,[2] M. P. Decowski,[4] E. Garcia,[7] N. George,[1] K. Gulbrandsen,[4] S. Gushue,[2] C. Halliwell,[6] G. A. Heintzelman,[2] C. Henderson,[4] R. Hołyński,[3] D. Hofman,[6] B. Holzman,[6] E. Johnson,[8] J. Kane,[4] J. Katzy,[4,6] N. Khan,[8] W. Kucewicz,[6] P. Kulinich,[4] W. T. Lin,[5] S. Manly,[8] D. McLeod,[6] J. Michałowski,[3] A. Mignerey,[7] J. Mülmenstädt,[4] R. Nouicer,[6] A. Olszewski,[2,3] R. Pak,[2] I. C. Park,[8] H. Pernegger,[4] C. Reed,[4] L. P. Remsberg,[2] M. Reuter,[6] C. Roland,[4] G. Roland,[4] L. Rosenberg,[4] P. Sarin,[4] P. Sawicki,[3] W. Skulski,[8] S. G. Steadman,[4] G. S. F. Stephans,[4] P. Steinberg,[2] M. Stodulski,[3] A. Sukhanov,[2] J.-L. Tang,[5] R. Teng,[8] A. Trzupek,[3] C. Vale,[4] G. J. van Nieuwenhuizen,[4] R. Verdier,[4] B. Wadsworth,[4] F. L. H. Wolfs,[8] B. Wosiek,[3] K. Woźniak,[3] A. H. Wuosmaa,[1] and B. Wysłouch[4]

(PHOBOS Collaboration)

[1]*Physics Division, Argonne National Laboratory, Argonne, Illinois 60439-4843*
[2]*Chemistry and C-A Departments, Brookhaven National Laboratory, Upton, New York 11973-5000*
[3]*Institute of Nuclear Physics, Kraków, Poland*
[4]*Laboratory for Nuclear Science, Massachusetts Institute of Technology, Cambridge, Massachusetts 02139-4307*
[5]*Department of Physics, National Central University, Chung-Li, Taiwan*
[6]*Department of Physics, University of Illinois at Chicago, Chicago, Illinois 60607-7059*
[7]*Department of Chemistry, University of Maryland, College Park, Maryland 20742*
[8]*Department of Physics and Astronomy, University of Rochester, Rochester, New York 14627*

(Received 17 April 2001; published 15 August 2001)

We have measured the ratios of antiparticles to particles for charged pions, kaons, and protons near mid-rapidity in central Au + Au collisions at $\sqrt{s_{NN}} = 130$ GeV. We observe $\langle \pi^- \rangle / \langle \pi^+ \rangle = 1.00 \pm 0.01(\text{stat}) \pm 0.02(\text{syst})$, $\langle K^- \rangle / \langle K^+ \rangle = 0.91 \pm 0.07(\text{stat}) \pm 0.06(\text{syst})$, and $\langle \overline{p} \rangle / \langle p \rangle = 0.60 \pm 0.04(\text{stat}) \pm 0.06(\text{syst})$. The $\langle K^- \rangle / \langle K^+ \rangle$ and $\langle \overline{p} \rangle / \langle p \rangle$ ratios give a consistent estimate of the baryo-chemical potential μ_B of 45 MeV, a factor of 5–6 smaller than in central Pb + Pb collisions at $\sqrt{s_{NN}} = 17.2$ GeV.

DOI: 10.1103/PhysRevLett.87.102301 PACS numbers: 25.75.–q

In this paper multiplicity ratios of antiparticles to particles for primary charged pions, kaons, and protons are presented for collisions of gold nuclei at an energy of $\sqrt{s_{NN}} = 130$ GeV. The data were taken with the PHOBOS detector during the first run of the Relativistic Heavy-Ion Collider (RHIC) at Brookhaven National Laboratory. The experiments at RHIC aim at understanding the behavior of strongly interacting matter at high temperature and density. Quantum chromodynamics, the fundamental theory of strong interactions, predicts that under these conditions a new state of matter will be formed, the quark-gluon plasma [1].

One of the most intriguing results from heavy-ion collisions at lower energies was the observation that particle ratios for particles with production cross sections varying by several orders of magnitude could be described in a statistical picture of particle production assuming chemical equilibrium [2–4]. This is particularly remarkable for the production rates of rare baryons and antibaryons containing multiple strange quarks [5], which were found to be difficult to reproduce in microscopic hadronic transport models [6,7]. One of the key ingredients for the statistical particle production picture is the baryo-chemical potential μ_B, which can be extracted from the $\langle K^- \rangle / \langle K^+ \rangle$ and $\langle \overline{p} \rangle / \langle p \rangle$ ratios presented here.

The data reported here were collected using the PHOBOS two-arm magnetic spectrometer. Details of the setup can be found elsewhere [8–10]. One arm (SPECP) of the spectrometer was only partially equipped with six layers of silicon sensors, providing tracking only in the field-free region close to the beam pipe. The other arm (SPECN) had a total of 16 layers of sensors, providing tracking both outside and inside the 2 T field of the PHOBOS magnet. For this analysis, only the central region of SPECN was used, covering $\pm 15°$ around the 45° axis of the experiment in the horizontal plane. Particles within this geometrical acceptance region typically traversed 13 silicon layers. A two layer silicon detector (VTX) covering $|\eta| < 1.5$ and 25% of the azimuthal angle provided additional information on the position of the primary collision vertex.

The primary event trigger was provided by two sets of 16 scintillator paddle counters covering pseudorapidities $3 < |\eta| < 4.5$. Additional information for event selection was obtained from two zero-degree calorimeters measuring spectator neutrons. Details of the event selection and centrality determination can be found in [11,12]. Monte Carlo (MC) simulations of the apparatus were based on the HIJING event generator [13] and the GEANT 3.21 simulation package, folding in the signal response for scintillator counters and silicon sensors.

For this analysis the 12% events with the highest signal in the paddle counters were selected, corresponding to the collisions with the highest number of participating nucleons N_{part}. The average number of participants for the selected events was estimated as $\langle N_{\text{part}} \rangle = 312 \pm 10(\text{syst})$, using a Glauber calculation relating N_{part} to the fractional cross section observed in bins of the paddle signal [11,12].

As the geometrical layout of the PHOBOS detector leads to an asymmetry in the acceptance and detection efficiency for positively and negatively charged particles for a given magnet polarity, data were taken using both magnet polarities (BPLUS and BMINUS). The reproducibility of the absolute field strength was found to be better than 1%, based on Hall probe measurements for each polarity and the comparison of mass distributions for identified particles for the two polarities.

The trigger event selection was checked using the number of reconstructed straight line particle tracks outside the magnetic field. These numbers agreed to within 0.2% for the BPLUS and BMINUS data sets.

Only events with a reconstructed primary vertex position between -16 cm $< z_{\text{vtx}} < 10$ cm along the beam axis were selected, thus restricting the incident angles of the tracks in the first few spectrometer planes. This optimizes the precision of the vertex determination and is essential for this analysis, as the distance of closest approach of each reconstructed track with respect to the primary vertex (dca_{vtx}) is the only tool for rejecting background particles from decays and secondary interactions. By requiring a consistent vertex position from the SPEC and VTX subdetectors, in combination with the known position of the beam orbit, a vertex resolution better than 0.3 mm (rms) in y and z directions and better than 0.5 mm in x direction was achieved.

Tracks in the spectrometer were found as follows: tracks in the first six layers outside the magnetic field were reconstructed by a road-following algorithm. Inside the field, two-hit combinations on consecutive layers were mapped into $(1/p, \Theta)$ space, where Θ is the polar angle at the primary interaction vertex and p the total momentum. A clustering algorithm then selected combinations of matching hits in $(1/p, \Theta)$ space, yielding track pieces inside the field. For track pieces inside and outside the field, the specific ionization dE/dx was calculated using the truncated mean of the angle-corrected hit energies, discarding the two highest energy values.

Straight and curved track pieces were then matched based on Θ, a fit to the combined track in the yz plane and requiring consistency in the independently determined dE/dx values. Accepted tracks were required to have five or more hits in the field-free region and six hits inside the field.

For the combined tracks the dE/dx was again calculated, discarding the four highest energy values. Particle identification was performed using p and dE/dx, which depends only on particle velocity. The identification cuts are shown in Fig. 1 with three bands corresponding to pions, kaons, and protons.

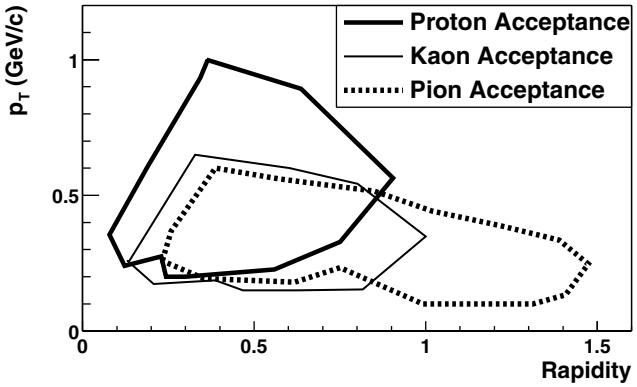

FIG. 1. Distribution of average energy loss as a function of reconstructed particle momentum. Three clear bands can be seen, corresponding to pions, kaons, and protons. The solid lines indicate the cut regions for counting identified particles.

The corresponding acceptance regions for identified particles in transverse momentum p_T and rapidity are shown in Fig. 2. The acceptance ranges in p_T are 0.1 to 0.6 GeV/c for $\pi^{+,-}$, 0.15 to 0.65 GeV/c for $K^{+,-}$, and 0.2 to 1.0 GeV/c for $p, \overline{p}$. Table I gives the resulting event and identified particle statistics for all combinations of magnet polarity, particle charge, and particle mass. Using two magnetic field settings allows the determination of two statistically independent values for each of the three particle ratios. As can be calculated from the numbers in Table I, the two values agree within statistical uncertainty for each of the ratios. Table I also shows the average transverse momentum $\langle p_T \rangle$ of the particles in the spectrometer acceptance. The average transverse momenta of corresponding particle and antiparticle selections agree within statistical error. Also, the average rapidity and the second moments of p_T and y distributions for accepted particles and antiparticles agree within errors. This shows that momentum distributions for particles and antiparticles in the PHOBOS acceptance range are similar and no acceptance correction is necessary for taking the ratios.

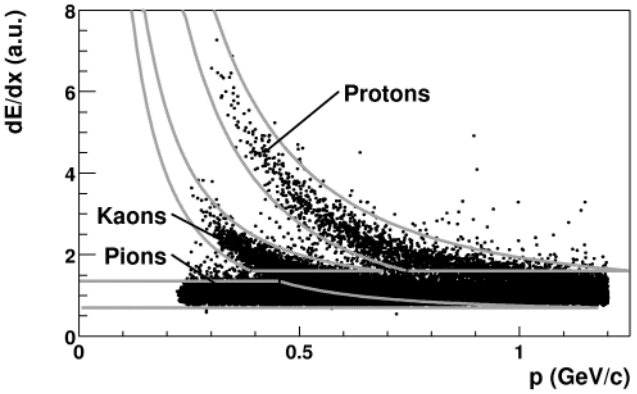

FIG. 2. Acceptance of the spectrometer as a function of transverse momentum and rapidity for pions, kaons, and protons. The acceptance is averaged over the accepted vertex range and azimuthal angle ϕ.

TABLE I. Number of accepted events, uncorrected number of identified particles, and uncorrected $\langle p_T \rangle$ for each magnetic field polarity.

	BPLUS 26 509 events		BMINUS 41 850 events	
	No. of particles	$\langle p_T \rangle$ (MeV/c)	No. of particles	$\langle p_T \rangle$ (MeV/c)
π^+	6208	412 ± 1	23 223	254 ± 1
π^-	14 783	253 ± 1	9679	410 ± 1
K^+	136	358 ± 4	256	248 ± 4
K^-	146	255 ± 5	198	366 ± 4
p	223	581 ± 10	331	475 ± 8
$\overline{p}$	109	481 ± 12	218	560 ± 8

The contamination of the proton and kaon samples was checked by testing the stability of the particle ratios against variation of the particle-ID cuts shown in Fig. 1. Within statistical error the ratios were stable against further changes of the cuts.

For comparison with data from other experiments and theoretical calculations, the particle ratios have to be corrected for particles produced in secondary interactions, loss of particles due to absorption in detector material, and feed-down particles from weak decays. Simulations show that the difference in contamination of π^+ and π^- by e^+ and e^-, which cannot be rejected by the dE/dx measurement, is negligible.

The acceptance for secondary and feed-down particles is limited to those produced within 10 cm radial distance from the primary collision vertex, as accepted tracks were required to have at least one hit in the first two layers of the spectrometer. The contamination is further reduced by requiring tracks to have $dca_{\rm vtx} < 3.5$ mm.

The contribution from secondary interactions, estimated using our MC simulation, is shown in Fig. 3 as a function of p_T. The net correction is 0.01 for $\langle \overline{p} \rangle / \langle p \rangle$ and much less than 1% for pions and kaons. As the MC reproduces the charged particle multiplicity near mid-rapidity to within 10%, we estimate a systematical uncertainty of this correction of less than 0.005.

The difference in absorption for protons and antiprotons in the detector material was studied based on GEANT simulations. The fraction of absorbed protons and antiprotons as a function of p_T is also shown in Fig. 3. From this correction, which averages to 1.7% for the protons and 6.3% for the antiprotons, a correction to $\langle \overline{p} \rangle / \langle p \rangle$ of 0.04 is obtained.

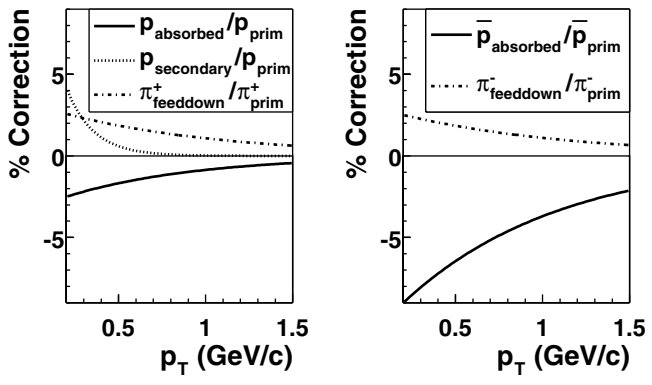

FIG. 3. Correction factors for particle multiplicities as a function of transverse momentum p_T for positive and negative particles. Correction factors of less than 1% and the p_T-independent feed-down correction for $\langle \overline{p} \rangle / \langle p \rangle$ are not shown.

The contribution from feed-down particles cannot be modeled as precisely, as the absolute yield of strange hadrons has not yet been measured at RHIC. Simulations show that the feed-down correction for $\langle K^- \rangle / \langle K^+ \rangle$ and $\langle \pi^- \rangle / \langle \pi^- \rangle$ (see Fig. 3) is less than 1%, whereas feed down to protons and antiprotons from Λ and $\overline{\Lambda}$ is not negligible. The feed-down correction to the $\langle \overline{p} \rangle / \langle p \rangle$ ratio can be evaluated as a function of the $\langle \overline{\Lambda} \rangle / \langle \Lambda \rangle$ and $\langle \Lambda \rangle / \langle p \rangle$ ratios. Transport model studies, as well as quark counting arguments and data from lower energies show that to a good approximation the following relationship holds [14]:

$$\frac{\langle \overline{\Lambda} \rangle}{\langle \Lambda \rangle} = \frac{\langle K^+ \rangle}{\langle K^- \rangle} \cdot \frac{\langle \overline{p} \rangle}{\langle p \rangle}.$$

Our data show $\langle K^+ \rangle / \langle K^- \rangle = 1.1$, suggesting only a 10% difference in $\langle \overline{\Lambda} \rangle / \langle \Lambda \rangle$ compared to $\langle \overline{p} \rangle / \langle p \rangle$. Using the $dca_{\rm vtx} < 3.5$ mm cut, less than half of the protons from weak decays are accepted in the analysis. This further reduces the feed-down correction to $\langle \overline{p} \rangle / \langle p \rangle$. Using MC simulations, the range of the correction was estimated by varying the $\langle \Lambda \rangle / \langle p \rangle$ ratio from 0.2, the value predicted by HIJING, to 0.4 and varying $\langle K^+ \rangle / \langle K^- \rangle$ from 1 to 1.2. The resulting correction to $\langle \overline{p} \rangle / \langle p \rangle$ ranges from 0 to -0.03, with a most probable value of -0.01. Our own $p/\overline{p}$ data (see Table I), as well as data from lower energies and MC simulation show that p_T distributions for baryons and antibaryons are very similar. The p_T dependence of the feed-down correction to the $\langle \overline{p} \rangle / \langle p \rangle$ ratio can therefore be assumed to be small and is neglected here.

After corrections we find the following ratios within our acceptance:

$$\langle \pi^- \rangle / \langle \pi^+ \rangle = 1.00 \pm 0.01(\text{stat}) \pm 0.02(\text{syst})$$
$$\langle K^- \rangle / \langle K^+ \rangle = 0.91 \pm 0.07(\text{stat}) \pm 0.06(\text{syst})$$
$$\langle \overline{p} \rangle / \langle p \rangle = 0.60 \pm 0.04(\text{stat}) \pm 0.06(\text{syst})$$

The results are in good agreement with data recently presented by the BRAHMS and PHENIX Collaborations [15] and STAR [16]. In Fig. 4 our results are compared to lower

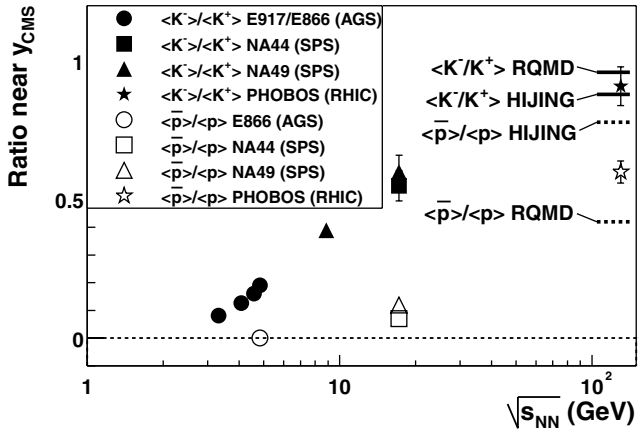

FIG. 4. $\langle K^- \rangle / \langle K^+ \rangle$ and $\langle \overline{p} \rangle / \langle p \rangle$ ratios as a function of $\sqrt{s}$ for nucleus-nucleus collisions, in comparison with predictions from the HIJING and RQMD models. Only statistical errors are shown.

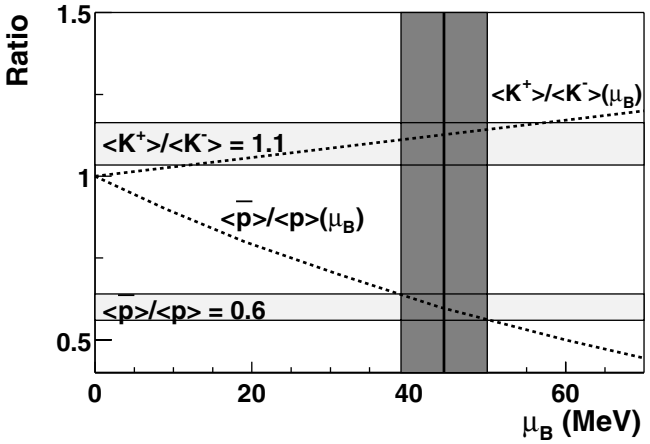

FIG. 5. Statistical model calculation (dotted lines) of $\langle K^+ \rangle / \langle K^- \rangle$ and $\langle \overline{p} \rangle / \langle p \rangle$ as a function of μ_B by Redlich *et al.* The horizontal bands show the ratios observed in the data (statistical errors only). The vertical shaded area indicates the allowed region in μ_B.

energy data [17–19] and calculations using the HIJING and RQMD [7] microscopic transport models. The values for the $\langle K^- \rangle / \langle K^+ \rangle$ and $\langle \overline{p} \rangle / \langle p \rangle$ ratios are significantly higher than at lower energies.

Using the same parameters that successfully described the charged particle multiplicity density in these collisions [11], HIJING overestimates $\langle \overline{p} \rangle / \langle p \rangle$ by 0.18. Clearly, the particle ratio data provide additional constraints for microscopic models. A better description may require a modification in the baryon number stopping mechanism, baryon-pair production or antibaryon annihilation.

An indication of possible mechanisms is given by the comparison with RQMD, which includes rescattering of produced hadrons and predicts a value for $\langle \overline{p} \rangle / \langle p \rangle$ that is 0.18 below our data. Both HIJING and RQMD agree within errors with the $\langle K^+ \rangle / \langle K^- \rangle$ measured by PHOBOS, with HIJING in the lower and RQMD in the upper range of the error band.

Finally, we estimate the baryo-chemical potential μ_B using a statistical model calculation [20] shown in Fig. 5. For a realistic range of chemical freeze-out temperatures of 160 to 170 MeV, both $\langle K^+ \rangle / \langle K^- \rangle$ and $\langle \overline{p} \rangle / \langle p \rangle$ are consistent with $\mu_B = 45 \pm 5$ MeV. This is much lower than the value of $\mu_B = 240$–270 MeV [3,4] obtained in statistical model fits to Pb + Pb data at $\sqrt{s_{NN}} = 17.2$ GeV, showing a closer but not yet complete approach to a baryon-free regime at RHIC.

This work was partially supported by U.S. DoE Grants No. DE-AC02-98CH10886, No. DE-FG02-93ER-404802, No. DE-FC02-94ER40818, No. DE-FG02-94ER40865, No. DE-FG02-99ER41099, and No. W-31-109-ENG-38, as well as by NSF Grants No. 9603486, No. 9722606, and No. 0072204. The Polish groups were partially supported by KBN Grant No. 2 P03B 04916. The NCU group was partially supported by NSC of Taiwan under Contract No. NSC 89-2112-M-008-024.

[1] See, e.g., J. P. Blaizot, Nucl. Phys. **A661**, 3 (1999).
[2] E. Schnedermann, J. Sollfrank, and U. Heinz, Phys. Rev. C **48**, 2462 (1993).
[3] F. Becattini, Z. Phys. C **69**, 485 (1996).
[4] P. Braun-Munzinger, I. Heppe, and J. Stachel, Phys. Lett. B **465**, 15 (1999).
[5] P. Koch, B. Müller, and J. Rafelski, Phys. Rep. C **142**, 167 (1986).
[6] S. A. Bass *et al.,* Prog. Part. Nucl. Phys. **42**, 313 (1998).
[7] H. Sorge, Phys. Rev. C **52**, 3291 (1995). We used version 2.4, including rope formation.
[8] B. Back *et al.,* Nucl. Phys. **A661**, 690 (1999).
[9] H. Pernegger *et al.,* Nucl. Instrum. Methods Phys. Res., Sect. A **419**, 549 (1998).
[10] PHOBOS Collaboration, R. Pak *et al.,* in Proceedings of Quark Matter '01 Conference (to be published).
[11] B. Back *et al.,* Phys. Rev. Lett. **85**, 3100 (2000).
[12] PHOBOS Collaboration, J. Katzy *et al.,* in Proceedings of Quark Matter '01 Conference (to be published).
[13] M. Gyulassy and X. N. Wang, Comput. Phys. Commun. **83**, 307 (1994). We used HIJING V1.35 with standard parameter settings.
[14] J. Zimanyi, Nucl. Phys. **A661**, 224 (1999).
[15] See Proceedings of Quark Matter '01 Conference (to be published).
[16] C. Adler *et al.,* Phys. Rev. Lett. **86**, 4778 (2001).
[17] L. Ahle *et al.,* Phys. Lett. B **490**, 53 (2000); Phys. Rev. C **60**, 064901 (1999); Phys. Rev. Lett. **81**, 2650 (1998).
[18] J. Bächler *et al.,* Nucl. Phys. **A661**, 45 (1999).
[19] I. G. Bearden *et al.,* Phys. Lett. B **388**, 431 (1996).
[20] K. Redlich, in Proceedings of Quark Matter '01 Conference (to be published).